

Mode-Locking between the Seasonal and the ENSO cycles

Carlos Hoyos*

*School of Earth and Atmospheric Sciences
Georgia Institute of Technology, Atlanta, GA 30332*

(Dated: December 11, 2003)

In this project the quasi-periodicity route to chaos emerging from a seasonally forced delay oscillator mechanism designed to study the El Niño - Southern Oscillation (ENSO) cycle is studied. Variety of atmospheric and oceanic observations show significant irregularity in the cycle. Different mechanisms have been proposed to explain the ENSO irregular behavior but there no agreement yet. The dynamical behavior of the delay oscillator is very similar to the one exhibited by the circle map when the strength of the nonlinear forcing is increased. In our simple model, the nonlinear parameter refers to the strength of the coupling between the ocean and the atmosphere. Numerical integrations of the delay equation suggest that the irregularity observed in ENSO is inherent to the nonlinear interaction between ocean and atmosphere together with the seasonal or annual forcing.

I. INTRODUCTION

The ENSO cycle (El Niño - Southern Oscillation) refers to the anomalous warming of the east equatorial Pacific Ocean, the weakening of the trade winds about and the changes in the Walker circulation about every 3.5 to 6 years. The role of the interaction between the ocean and the atmosphere in the tropical Pacific generating the ENSO cycle was first postulated by Bjerknes [1]. Bjerknes stated that anomalies in sea surface temperature in the Pacific cause the trade winds to strengthen or weaken and, driving changes in ocean circulation that produce anomalous sea surface temperatures. During normal conditions the trade winds blow towards the west across the tropical Pacific. The warm surface water is located at the west Pacific, which in average has a higher sea surface height (about 1/2 meter) at Indonesia than at Ecuador. The sea surface temperature is about 8 degrees C higher in the west, with cooler temperatures at the South American coast, due to an upwelling of cold and nutrient-rich water from deeper levels sustaining the biodiversity. Rainfall is found in rising air over the warmest water, and the east Pacific is relatively dry. During El Niño, the trade winds get weaker in the central and western Pacific occasioning a deepening of the thermocline close to South America, and an elevation of the thermocline in the west. This reduced the amount of upwelling, which normally cools the surface, and reduces the supply of nutrient-rich water to the surface. These conditions lead a rise in sea surface temperature and a reduction in the fisheries in this region (Figure 1). Also, the warm pool moves eastward and the rain-

fall follows it. The name “El Niño” was given by the Peruvian fishermen describing the warmer waters appearing at the Peru coast right after Christmas time, referring to Christ child. This is one of the features reflecting the coupling between ENSO and the annual cycle. Also, there is a “predictability barrier” which statistically refers to the loss of autocorrelation or persistence in the ENSO indexes that always occurs during the boreal spring.

Although the basic oscillatory aspects of ENSO are understood, the observed irregularity of the cycle remains unclear to the community. Several authors have postulated three main hypotheses for the source of ENSO irregularity [5–9, 11]: i) long-term variation of the climatic background state; ii) uncoupled atmospheric weather (stochastic) noise; iii) deterministic chaos within arising from nonlinear dynamics of the coupled system. In this paper, we concentrate the analysis on the last source of irregularity, following the work of Tziperman et al. [11], by studying the quasi-periodicity route to chaos that appears as the nonlinearity in a forced delay oscillator model is increased. The first step to accomplish the objective is to review the first part of Jensen et al. [4], as well as the chapter “Irrationally Winding” in [2] on mode-locking in circle maps, as a basis of our study of the resonant response occurring in systems of coupled oscillators, or oscillators coupled to periodic external forcing.

In the following section the basics of the dynamics resulting from circle map is reviewed, including the construction of the Arnold’s tongues and the devil’s staircase. In section III the mechanism of the delay oscillator for ENSO is explained and a simple model for the Kelvin and Rossby wave dynamics with annual forcing is introduced. Details of integration of the forced delayed equation are also presented. Section IV is dedicated to present the results of the integration for several different κ s (strength of the nonlinearity) in order to explore

*choyos@eas.gatech.edu

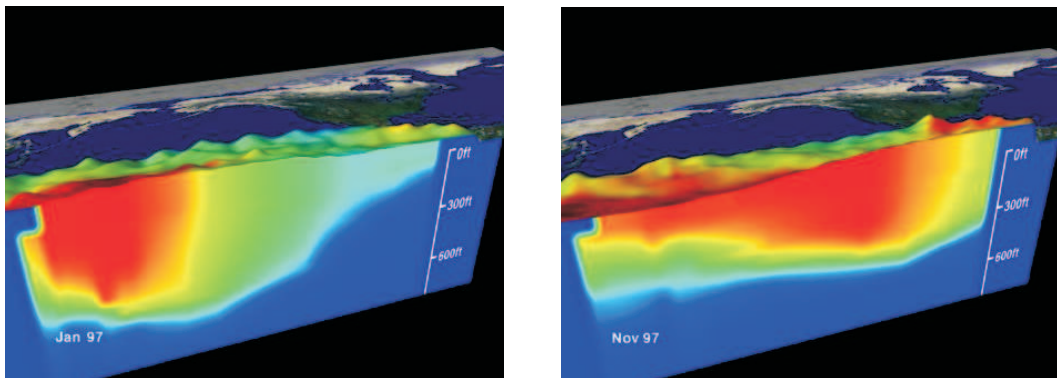


FIG. 1: Vertical slice of the Pacific Ocean trough the equator. Left: Normal conditions. Right: El Niño conditions (source: www.pmel.noaa.gov).

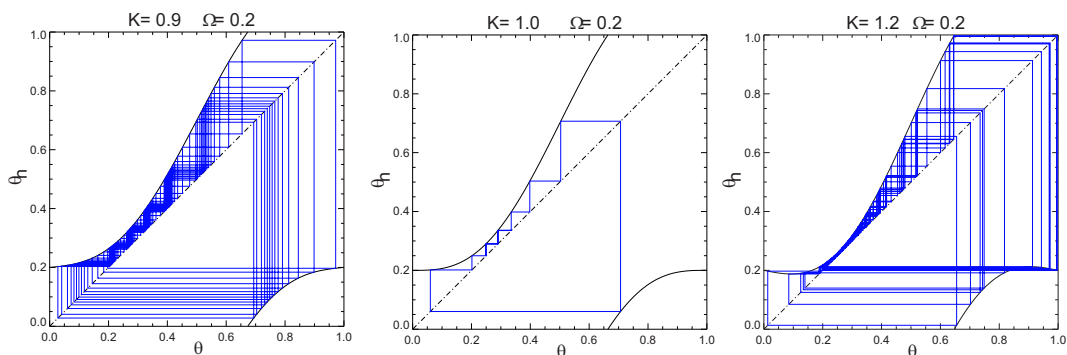


FIG. 2: Iterations of the circle map for $\Omega = 0.2$ and $K = 0.9, 1.0,$ and 1.2 .

the quasi-periodicity route to chaos. Different diagnostics, like reconstruction of the phase space, return maps, and power spectrum are used to examine the obtained time series. A diagram similar to the devil's staircase is constructed. Section V presents some concluding remarks.

II. CIRCLE MAP

The circle map is a one-dimensional map which maps a circle onto itself. The circle map exhibits quasi-periodicity route to chaos, which occurs in periodically forced nonlinear systems. One specific circle map, the sine map, is defined as follows

$$\Theta_{n+1} = \Theta_n + \Omega - \frac{K}{2\pi} \sin(2\pi\Theta_n) \pmod{1}, \quad (1)$$

where Θ_{n+1} is an angle denoting the location of the n th iteration on the circle, and Ω represents the frequency of the system when $K = 0$. The sine map is nonlinear, with the strength of non-linearity parameterized by parameter K . In this

case, the quasi-periodicity route to chaos can be investigated in the two-parameter plane K and Ω . Studying the circle map help us understand how resonances occur when the frequency of a harmonic Pw_1 of one oscillator, approaches some harmonic Qw_2 of another oscillator. In the resonant region the frequencies of the two oscillators lock into the rational ratio P/Q . The nonlinear couplings and the overlap of resonant regions eventually lead to chaotic behavior. Evolutions of iterations of the circle map for different parameters is presented in Figure 2. When $0 < K < 1$, the map is monotonic and the winding number, defined as

$$W = \lim_{n \rightarrow \infty} \frac{1}{n} (\Theta_n - \Theta). \quad (2)$$

and representing the mean number of cycles per iteration, locks at every rational P/Q in finite non-zero intervals of Ω . When $0 < K < 1$ the behavior is periodic and quasi-periodic. At $K = 1$, the map develops a singularity at $\Theta = 0$, and almost all the initial conditions evolve into periodic orbits. For $K > 1$ the map is not monotonic anymore, i.e. non-invertible, resulting in chaotic trajectories.

Figure 3 shows the winding number W vs Ω for different K s and some specific P/Q (Figure 3). The width of the lines represents the size of the locking intervals and they might be interpreted as the probability of being in a locked region if Ω is selected randomly. When K is close to zero, the chances of W being a rational are very low, while when $K = 1$ the probability is almost 1. Figure 4 shows the $K - \Omega$ diagram for different values of P/Q , showing the boundaries of the locking regions. This diagram is known as Arnold's tongues. Figure 5 presents the winding number W at $K = 1$ also known as the devil's staircase. Above $K = 1$, the regions of resonance overlap generating and chaotic behavior since the system jumps erratically between the competing resonances.

III. DELAY OSCILLATOR MODEL

Although much of the details of ENSO and its connection to the global climate remain unknown, the basic dynamics can be explained in terms of the "delayed oscillator" idea [10]. This idea is based on the assumption that the strongest coupling between the ocean and the atmosphere takes place in the middle of the Pacific equatorial basin, and it suggests that wind anomalies introduced by sea surface temperature (SST) changes in the center of the Pacific generate a downwelling wave in the thermocline that travels eastward to the South American coast as a Kelvin wave (onset of El Niño) and westward propagating Rossby wave on the thermocline. The Rossby waves are reflected from the western boundary of the Pacific Ocean as upwelling Kelvin waves which travel eastward to balance the downwelling Kelvin waves, ultimately terminating the El Niño event (Figure 6).

Different authors have proposed different mathe-

matical "toy models" for the delay oscillator, some of them directly derived from the barotropic mode of a simple two layer model. As the main objective of this project is to study the phase-locking between the annual and the ENSO cycles, we are going to base our numerical experiments in the following delay equation proposed by Tziperman et. al. [11]

$$\frac{dh(t)}{dt} = c_1 A \left(h \left(t - \frac{L}{2C_K} \right) \right) - c_2 A \left(h \left(t - \frac{L}{C_K} - \frac{L}{2C_R} \right) \right) + c_3 \cos(\omega_a t), \quad (3)$$

where $h(t)$ represents the thermocline depth deviations from seasonal depth values at the eastern boundary, t is time, L is the Pacific basin width, ω_a is the annual frequency of the idealized seasonal forcing. The first term of the right represents the wind-forced Kelvin mode travelling at speed C_K to the eastern boundary. The wave is generated at the middle of the basin, taking $\frac{L}{2C_K}$ time to reach the boundary. The second term represents the westward-travelling Rossby wave of speed C_R excited by the wind at time $t - \frac{L}{C_K} - \frac{L}{2C_R}$, and is reflected as a Kelvin wave. The Pacific basin width at the equator is about $L \sim 16000\text{km}$, and the typical speed of a Kelvin wave is about $C_K \sim 2.4\text{m/s}$. Rossby waves travel at approximately 1/3 of the speed of a Kelvin wave. The selection of reasonable values must lead to $\frac{L}{C_K} \sim 2.3 - 2.5$ months.

The function $A(h)$ relates wind stress to SST and SST to thermocline depth. Here we are going to use the function proposed by Münnich et al. [7] which was fashioned after the shape of the Tropical thermocline

$$A(h) = \begin{cases} b_+ + \frac{b_+}{a_+} \left\{ \tanh \left[\frac{\kappa a_+}{b_+} (h - h_+) \right] - 1 \right\} & , \quad h_+ < h \\ \kappa h & , \quad h_- \leq h \leq h_+ \\ -b_- - \frac{b_-}{a_-} \left\{ \tanh \left[\frac{\kappa a_-}{b_-} (h - h_-) \right] - 1 \right\} & , \quad h < h_- \end{cases} \quad (4)$$

In the equation we have $a_{\pm} > 1$ and

$$\begin{aligned} h_+ &= \frac{b_+}{\kappa a_+} (a_+ - 1) \\ h_- &= \frac{-b_-}{\kappa a_-} (a_- - 1), \end{aligned} \quad (5)$$

κ parameterized the strength of the nonlinearity. Here the nonlinearity is given by the variation of the strength of the coupling with h . Selection of the values for all parameters will be shown at section IV. To integrate equation 3 we use a fourth order RungeKutta scheme with fixed step size, ap-

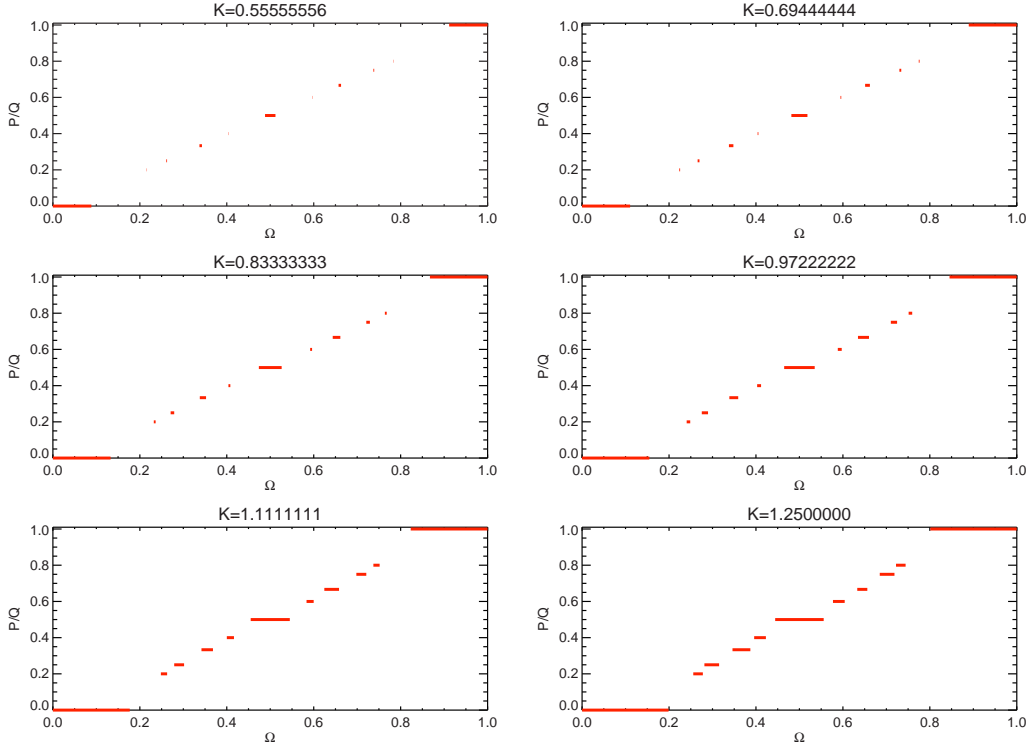


FIG. 3: Winding number W vs Ω for different K and at $P/Q = 0, 1/5, 1/4, 1/3, 2/5, 1/2, 3/5, 2/3, 3/4, 4/5, 1$.

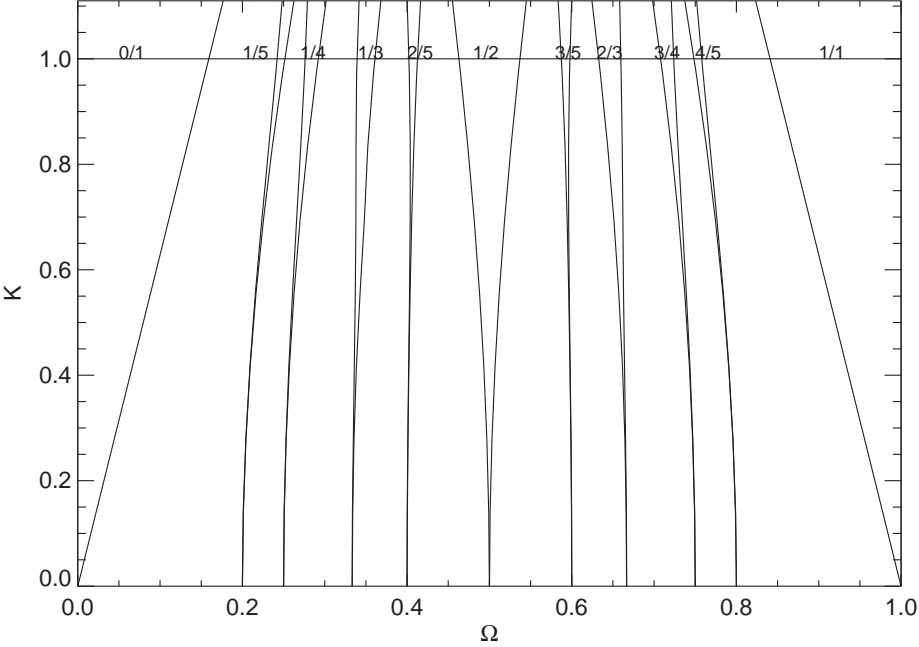


FIG. 4: K - Ω diagram for the circle map (Arnold tongues).

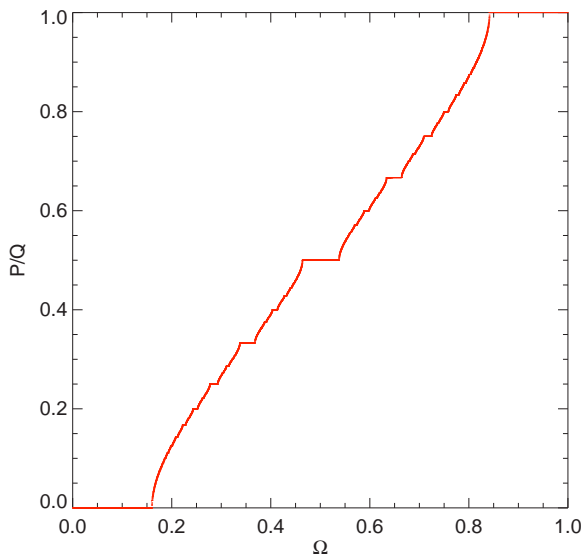


FIG. 5: Winding number W vs Ω for the circle map with $K = 1$ (Devil's staircase).

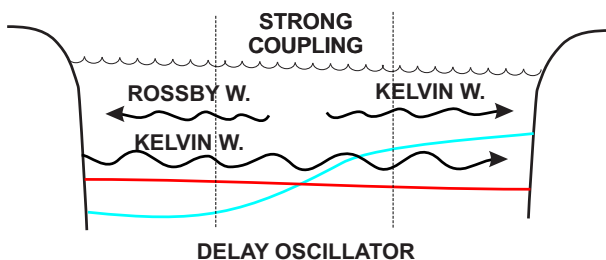


FIG. 6: Sketch of the delayed oscillator mechanism.

appropriately modified to account for delay [3].

A. Integration of the delay equation

Our original system is of the form

$$\frac{dh(t)}{dt} = f(h(t - T_1), h(t - T_2), t) \quad (6)$$

with $T_2 > T_1 > 0$. Recall the fourth order Runge-Kutta scheme with fixed step size s for the system $\dot{h}(t) = f(h(t), t)$, involves the evaluation of

$$\begin{aligned} k_1 &= sf(h_n, t_n), \\ k_2 &= sf\left(h_n + \frac{k_1}{2}, t_n + \frac{s}{2}\right), \\ k_3 &= sf\left(h_n + \frac{k_2}{2}, t_n + \frac{s}{2}\right), \\ k_4 &= sf(h_n + k_3, t_n + s) \end{aligned} \quad (7)$$

in order to compute $h_{n+1} = h_n + \frac{k_1}{6} + \frac{k_2}{3} + \frac{k_3}{3} + \frac{k_4}{6} + O(s^5)$. In our delay case, using the notation $h_{n-\frac{\tau_1}{s}} \equiv h(t_n - T_1)$ with $T_1 = sm$ for some integer m (similar for T_2), we need to evaluate

$$\begin{aligned} k_1 &= sf\left(h_{n-\frac{\tau_1}{s}}, h_{n-\frac{\tau_2}{s}}, t_n\right), \\ k_2 &= sf\left(\frac{h_{n-\frac{\tau_1}{s}} + h_{n+1-\frac{\tau_1}{s}}}{2}, \frac{h_{n-\frac{\tau_2}{s}} + h_{n+1-\frac{\tau_2}{s}}}{2}, t_n + \frac{s}{2}\right), \\ k_3 &= sf\left(\frac{h_{n-\frac{\tau_1}{s}} + h_{n+1-\frac{\tau_1}{s}}}{2}, \frac{h_{n-\frac{\tau_2}{s}} + h_{n+1-\frac{\tau_2}{s}}}{2}, t_n + \frac{s}{2}\right), \\ k_4 &= sf\left(h_{n+1-\frac{\tau_1}{s}}, h_{n+1-\frac{\tau_2}{s}}, t_n + \frac{s}{2}\right), \end{aligned} \quad (8)$$

Note that the evaluation of k_2 and k_3 requires the evaluation of $h(t)$ at midpoints of intervals defined by our time step. Here this evaluation is approximated using linear interpolation, or which is the same, the average of $h_{n-\frac{\tau_1}{s}}$ and $h_{n+1-\frac{\tau_1}{s}}$ (same for T_2).

The slow dynamics resulting from equation 3 remains unchanged if we use time steps smaller than 10 days.

IV. RESULTS

Since the main objective of the paper is to study the quasi-periodicity route to chaos that appears from equation 3 as the nonlinearity is increased, the only parameter that changes in the integration is κ . We need to select reasonable values for all parameters that would remain fixed throughout the integrations. It is important to note that the idea is to be able to study the general and most basic dynamics arising from the delay mechanism rather than having $h(t)$ close to the observations. In other words, here the resemblance of the power spectrum of $h(t)$ to the one computed from observations is more important than the actual values of $h(t)$. In fact, the magnitude of the output is easily controllable by the parameters in equation 4, but the actual dynamics depends more on the relationship between parameters than their gross values.

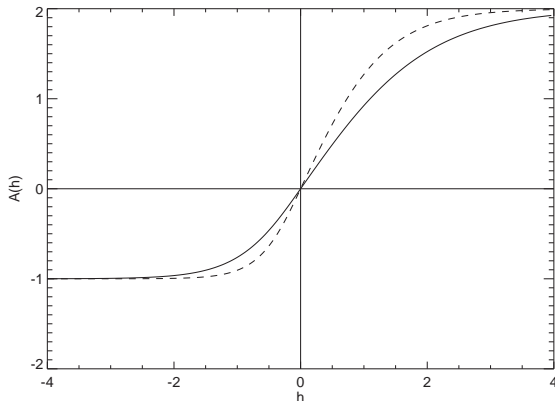


FIG. 7: Forcing function $A(h)$ given in Eq. 4.

In the integrations, L/C_K was set to 72 days and L/C_R to 216 days. Following Tziperman et al. [11] $c_1 = 1/180$, $c_2 = 1/120$, and $c_3 = 1/138$. To obtain good power spectra, $a_+ = 1$, $a_- = 1$, $b_+ = 2$, $b_- = -1$. Figure 7 shows $A(h)$ for $\kappa = 1$ (solid line) and $\kappa = 1.5$ (dashed line). A second set of integrations was performed using $L/C_K = 69$, $L/C_R = 207$, and $b_- = -0.4$.

Using the selected parameters, 75 runs for different values of κ were performed. The total integration period was 400 years for each run, and the time step used correspond to 5 days. First 50 years of integration were removed for the analysis. Figures 8 to 11 show some typical results of the integration. Figures 8 and 9 correspond to the first set of parameters, and they show the Fourier spectrum of the $h(t)$ time series (not show), the reconstructed phase space using sub-sampling with lag $\tau = 365$ days, and the return map calculated from the geometric center of each attractor (red line) and from the point $(0,0)$ in the reconstructed phase space (blue line). In general, the integration resulted in periodic, quasi-periodic and chaotic time series. For low values of κ ($\lesssim 0.9$), the atmosphere-ocean interaction is not strong enough to generate important Kelvin and Rossby waves and consequently the seasonal forcing dominates resulting in a single peaked Fourier spectrum at 1 year period. In the phase space this trajectory degenerates to a single point.

When the nonlinearity increases slightly (κ increases), a second significant period appears in the Fourier spectrum around 3.8-4 years. The new period is incommensurate with the annual cycle and corresponds to the natural frequency of the unforced delay oscillator for the equatorial Pacific case. Remember that the typical ENSO cycle is be-

tween 3.5 to 6 years. Both, the phase space, which is a simple closed loop, and the return map become very similar to those for the circle map (see Section II). The motion is irregular but not chaotic. If κ increases further, the loop in the phase space deforms according to the new but not dominant periods seen in the Fourier spectrum. The dominant period is in all cases between 3.5 and 4 years.

Note that when the return map is estimated using the geometric center, the results are better in general than when using $(0,0)$ as the center. When $(0,0)$ is “outside” of the attractor the return map is not useful at all. This comment is valid in general so from now on we will refer to the return map estimated from geometric center (red line in the Figures 8 to 11).

For stronger nonlinearity the system becomes mode-locked as in the circle map. The frequency of the delay oscillator adjust to a rational multiple of the seasonal forcing. The resulting time series is periodic. In Figure 9 there is an example where the delay oscillator and the annual forcing lock into a period 4 years. In the nonlinearity is big enough, the system becomes chaotic, the Fourier spectrum shows variance at all time scales, the phase space shows a strange attractor, and the return map is not monotonic anymore. In the first set of integrations, even for very high nonlinearity, the time series is very irregular but not quite chaotic, the phase space shows significant convex regions but is not folded yet, and the return map is very close to monotonic. Although it is not “fully chaotic”, this is the kind of irregularity seen in the data. In the second set of integrations a similar general response appears when increasing the nonlinearity. The main difference is that for high values of κ (e.g. $\kappa = 1.725, 2.0$) the phase space appears folded, and the return map develops a local minimum. In general, the reconstructed attractors are very thin; in other words, there is no interesting details when zooming into the plots.

Motivated by the great similarity between the dynamics observed in the circle map and the forced delay oscillator, and with the aim of construction a diagram similar to the Arnold’s tongues for our simple ENSO model, the estimated return map was fitted to cosine functions using Fourier transform such that

$$\Theta_{n+1} = \Theta_n + \Omega + \sum_i A_i \cos(2\pi\omega_i\Theta_n + \phi_i) \pmod{1}, \quad (9)$$

where ω_i are all the frequencies analyzed with the Fast Fourier Transform, A_i and ϕ_i are the corresponding amplitude and phase found with the FFT. Originally, only most important modes found with the FFT were used to fit the return map but

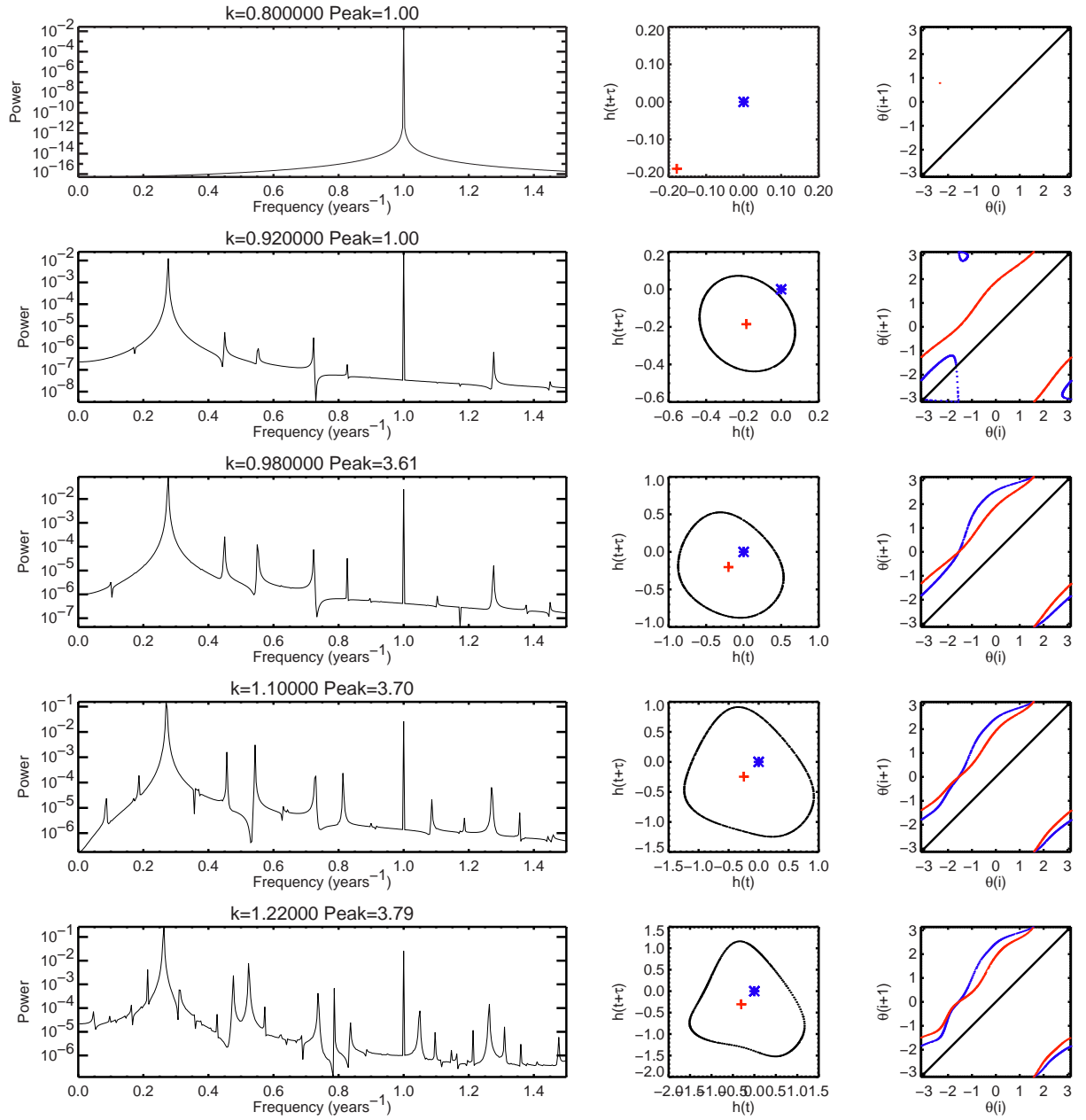


FIG. 8: Integration of the forced delay equation for the selected parameters and different values of κ . The left column shows the Fourier spectrum of each run. The corresponding κ and the period of the spectral maximum are shown in each spectrum. The center column shows the phase space reconstruction using $\tau = 365$ days. The blue star is at $(0,0)$ while the blue plus sign is at the geometric center of each attractor. The right column shows the corresponding return map, using both $(0,0)$ and the geometric center to compute the subtended angle.

in the majority of cases this introduced unrealistic local minima changing the dynamics of the map (see Figure 12). For that reason all Fourier modes were used. Figure 13 shows three fitting examples for different behaviors. The left plot correspond to a quasi-periodic behavior (first set of parameters,

$\kappa = 0.92$). In this kind of cases, the Fourier fitting is very good since the system visits all points in the attractor with almost equal likelihood. In the second case ($\kappa = 0.92$), the corresponding time series is very irregular but the return map is very close monotonic and the Fourier fitting works well.

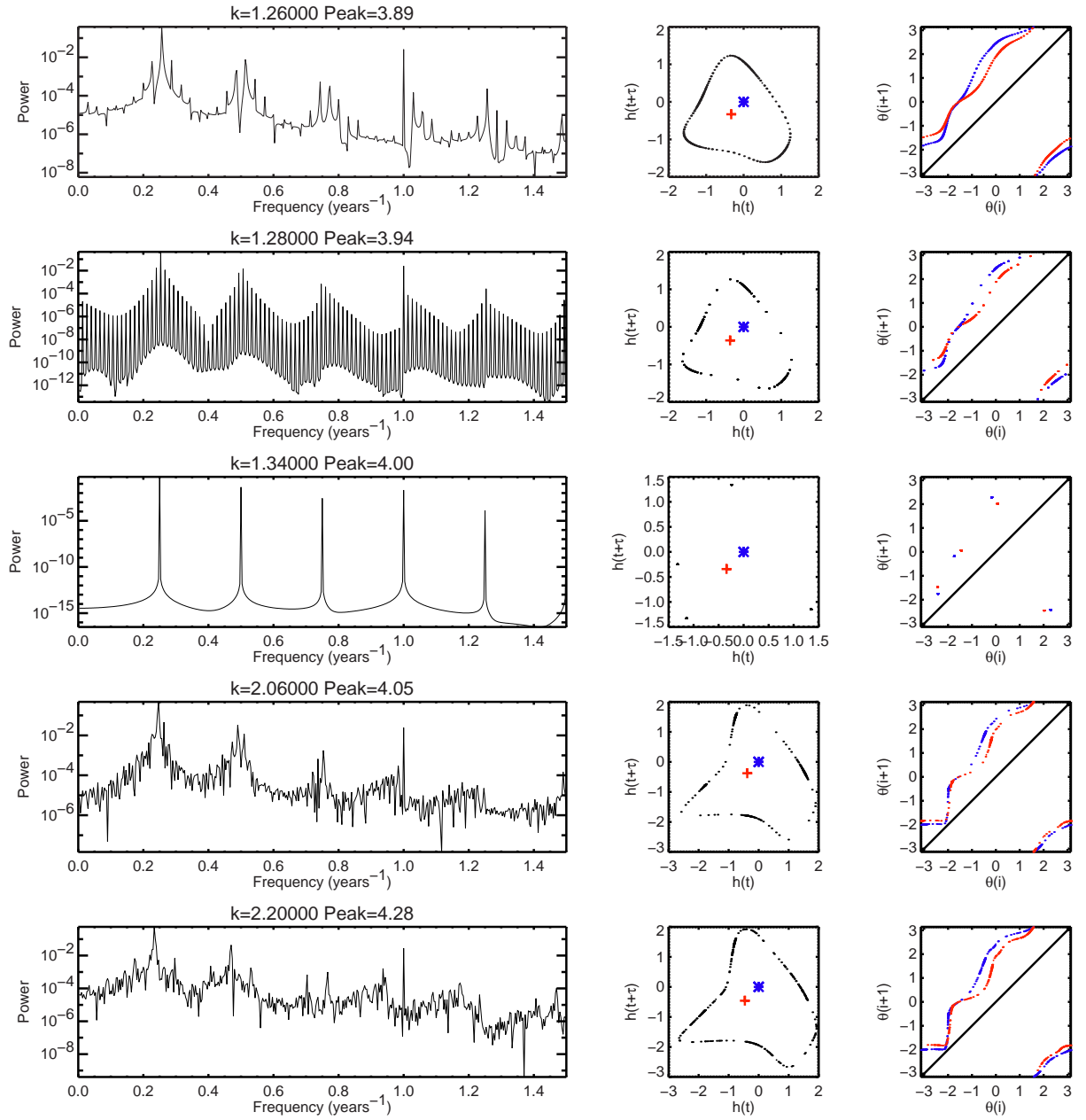


FIG. 9: Continuation of Figure 8.

However, it can be seen that the fitting is not as smooth as in the previous case and high frequency variability appears in the Fourier fitted map. The third case correspond to a chaotic time series with a non-smooth return map. The map is specially “noisy” between $\theta = 0.8$ and $\theta = 1$. and the fitting does not work well in this region.

After having the fitting functions for every κ value, we could explore periodic orbits by iterating the fitting function itself, and construct diagrams

similar to the devil’s staircase by changing Ω in equation 9. In general, Ω results as a combination of all parameters in function $A(h)$ and in the equation 3, which means changing Ω is similar to exploring the delay model in all domain of parameters, some of them not representative of ENSO cycle.

Figures 14 and 15 show two examples of return map iteration, one with $\kappa = 0.98$ and the other with $\kappa = 2.2$. In general, in the range of parameters

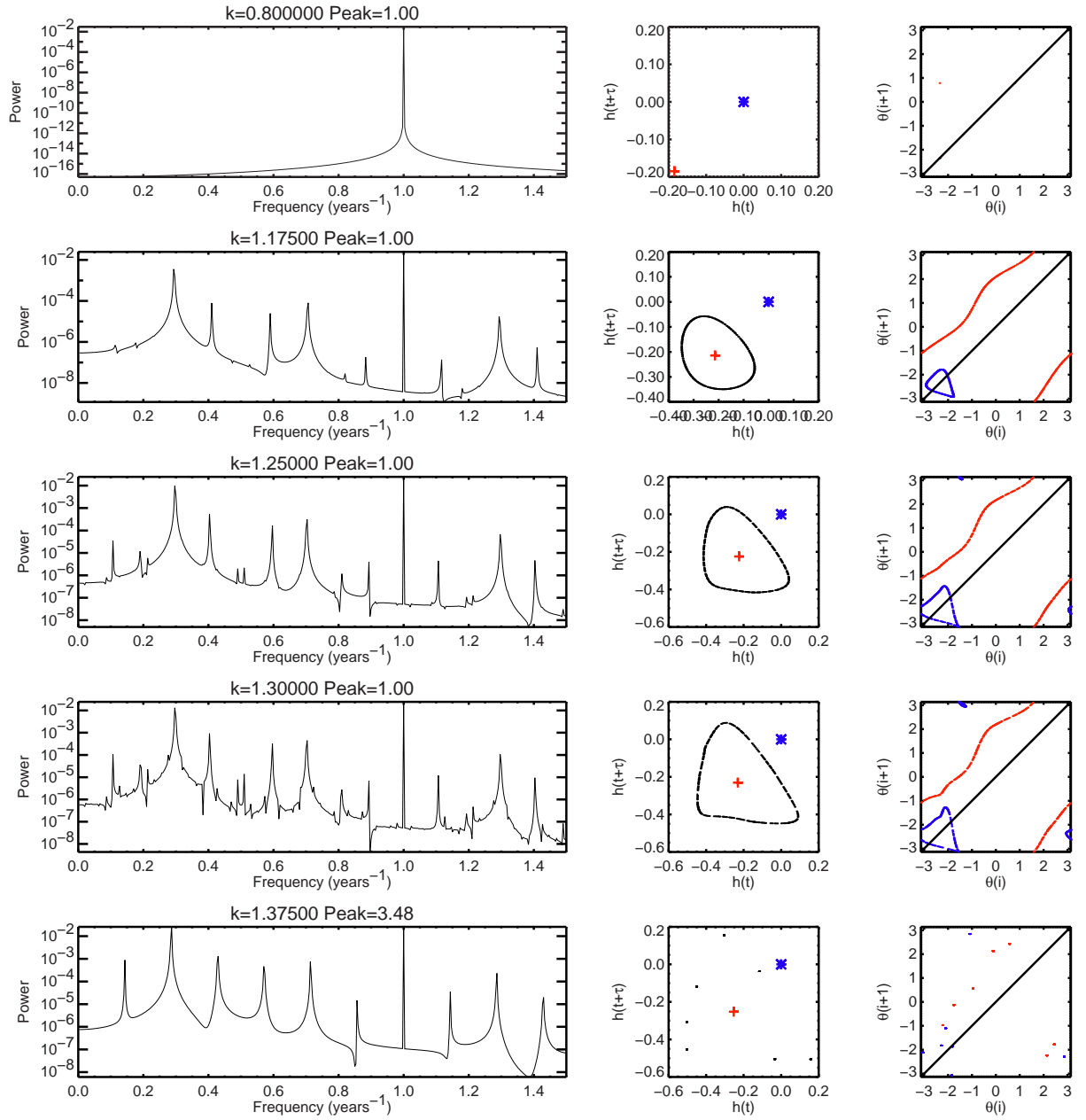


FIG. 10: Same of Figure 8 with second set of parameters ($L/C_K = 69$ days, $b_n = -0.4$).

representative of ENSO, when the map is smooth and monotonic there appear no single fixed when the map is iterated, but at some iteration the original map transforms into the $\theta_n = \theta_{n+1}$ line (see Figure 14). In return maps coming from very irregular time series, there is a significant deformation of the map, probably and artifact due to the high frequencies in the fitting. However, it can be seen that every multiple of 4, which is the dominant period of ENSO and the predominant period

in our test, the map becomes tangent or crosses the $\theta_n = \theta_{n+1}$ line.

Figure 16 shows the devil's staircases constructed from different values of κ by using the fitted return maps and changing ω . The winding number was computed as in equation 2. There is a strong similarity with the staircases coming from the circle map. The width of the steps increases as the nonlinearity increases. An important point is that the step in the diagrams that concern us

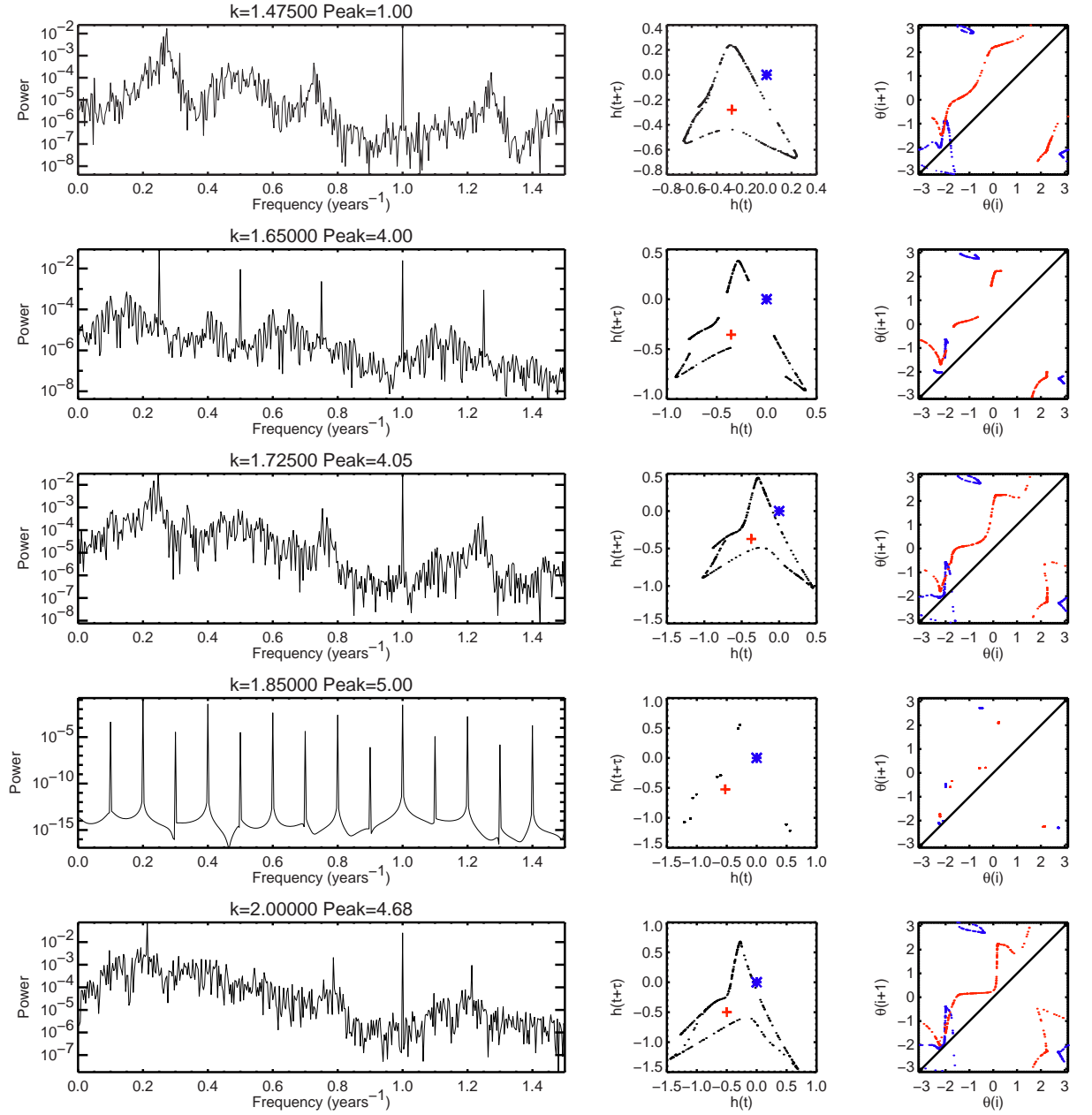


FIG. 11: Continuation of Figure 10.

(1/4) is very small compared to the other important steps. Other steps correspond to non realistic parameters for the Earth case. In that sense, they represent the locking in planets with wider oceanic basins, smaller seasonal forcing (orbital parameters), etc... In some of those unknown planets, the locking itself is more stable since the step is present for wider range of parameters here represented in Ω , giving “them” an advantage point towards prediction.

It has been suggested that the Madden-Julian Oscillation (MJO), which is the dominant component of the intraseasonal variability in the tropical atmosphere, may influence the tropical climate by modulating the timing and strength of El Niño events. As a simple test, here we introduced the MJO in our simple model by introducing a new term that generates every 30 days (typical MJO scale) pulse-like Kelvin waves at the west of the Pacific that travel all the basin to modify oceanic

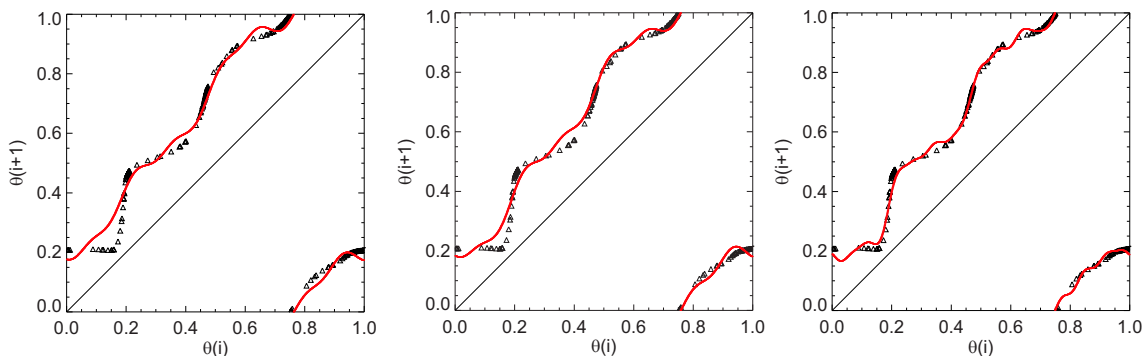


FIG. 12: Example of fitting using different number modes for $\kappa = 2.20$. Left: 3 modes. Center: 5 modes. Right: 15 modes.

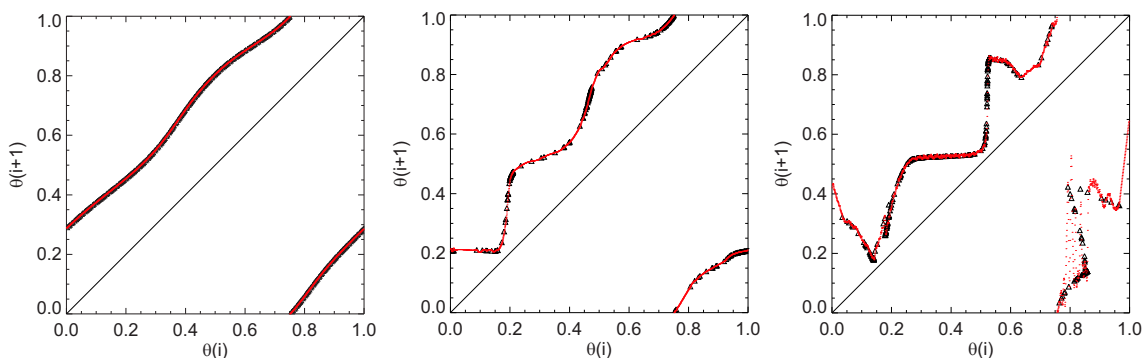


FIG. 13: Fourier fitting for different values of κ . Left: First set of parameters, $\kappa = 0.92$. Center: First set, $\kappa = 2.20$. Right: Second set, $\kappa = 2.0$.

conditions at the east side of the basin. Integrations were performed with the first set of parameters and the results for same values of κ as in Figures 8 and 9 are shown in Figures 17 and 18. It can be seen that the global behavior does not change, but longer periods than 4 years appear when the nonlinearity is increased. This fact is important in practice because according to the strength of an MJO, it can modify not only the strength of the following ENSO but also the dominant periodicity.

V. DISCUSSION

A simple nonlinear seasonally forced model of ENSO based on the delay oscillator hypothesis was introduced, and results numerical integration show the quasi-periodicity route to chaos appears when the nonlinearity, here representing the degree of ocean-atmosphere coupling, was increased. The dynamics is much similar to the one exhibit by the circle map. The parameters used in the in-

tegration intend to simulate the conditions of the tropical Pacific basin, and the resulting dominant period, aside from the annual cycle, corresponds to the observed ENSO cycle. This suggest that the periodicity and the observed ENSO irregularity is inherent to the wave delay dynamics and its mode-locking to the seasonal cycle.

The fact that the dominant periodicity changed when the MJO was included is practically important and it deserves a more careful analysis. This means that phenomena like MJO, that may be classified as weather noise, are not a key factor in the generating the observed ENSO irregularity but they do affect its timing and its strength.

Acknowledgments

I would like to thank Professors Predrag Cvitanović and Mason Porter for the helpful comments and suggestions.

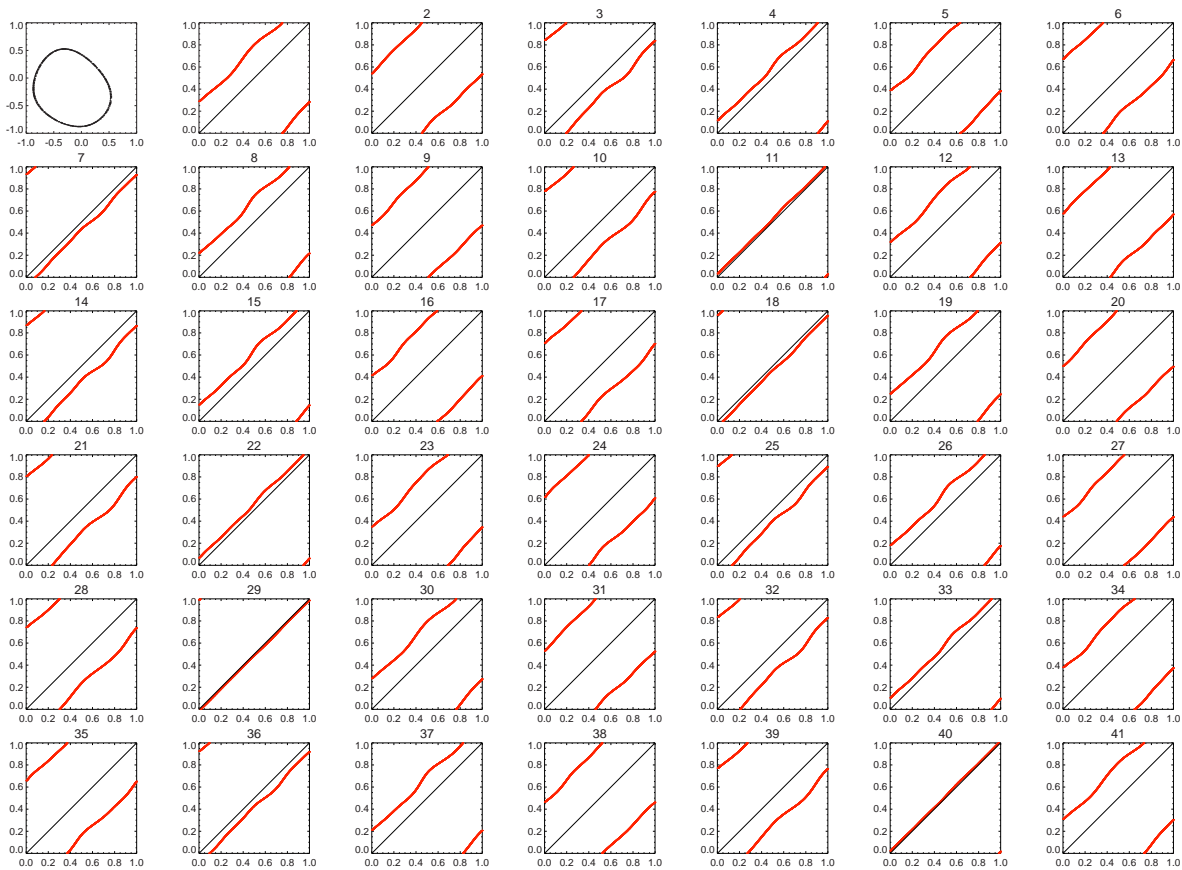


FIG. 14: Iteration of the return map for the first set of parameters and $\kappa = 0.98$.

APPENDIX A: ORIGINAL OUTLINE

Thu Oct 23 2003: Study of the Circle Map. Construction of Arnold tongues, devil's staircase. The code will be developed in IDL.

Thu Oct 30 2003: Integration of the forced delayed oscillator. Code in IDL or C depending of the efficiency of the algorithms.

Thu Nov 06 2003: Start construction of power spectra, reconstruction of the phase space, and return maps.

Thu Nov 13 2003: Finish the previous task and construct diagrams analogous to the Arnold tongues and the devil's staircase.

Thu Nov 20 2003: General review of the previous work. I expect to add and/or implement the ideas and suggestions arising from the interaction the professor and the class.

Thu Nov 27 2003: Write up of the results until this point. This completes the minimal realistic goals of the project. If possible, modify the forced delayed oscillator equation to include the MJO effects. Integrate the new equation

Thu Dec 04 2003: Compare the 2-oscillator route to chaos with the 3-oscillator case. Finish writing the main draft of the project.

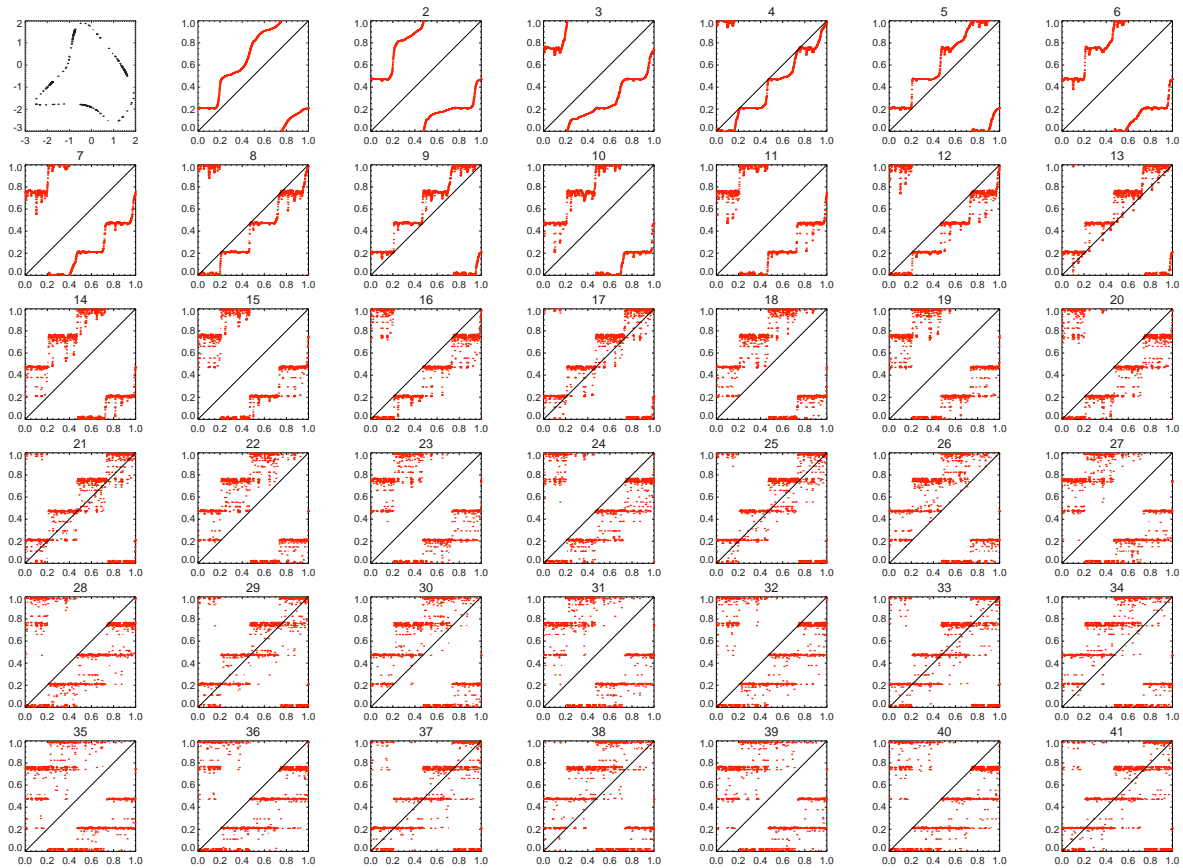
Thu Dec 11 2003: Term paper deadline.

[1] Bjerknæs, J., 1969: Atmospheric teleconnections from the equatorial Pacific. *Mon. Wea. Rev.*, 97, 163-172.

[2] Cvitanović P., R. Artuso, R. Mainieri, G. Tanner and G. Vattay, *Chaos: Classical and Quantum*,

chaosbook.org/ChaosBook/ (Niels Bohr Institute, Copenhagen 2003)

[3] Hairer, E., S. P. Nørsett, G. and Wanner, 1987: *Solving Ordinary Differential Equations I: Nonstiff Problems*, Springer-Verlag, Berlin.

FIG. 15: Same as 14 for $\kappa = 2.2$.

- [4] Jensen, M. H., P. Bak, and T. Bohr, 1984: Transition to chaos by interaction of resonances in dissipative systems. I. Circle maps. *Phys. Rev. A*, 30, 1960.
- [5] Kleeman, R. and A. M. Moore, 1997: A theory for the limitation of ENSO predictability due to stochastic atmospheric transients. *J. Atmos. Sci.*, 54: 753767.
- [6] Jin, F.-F., J. D. Neelin and M. Ghil 1994: El Nio on the devil's staircase: annual subharmonic steps to chaos. *Science*, 264, 70-72.
- [7] Münnich, M., M. A. Cane, and S. E. Zebiak, 1991: A study of self-excited oscillations in the tropical ocean atmosphere system. part II: Nonlinear cases. *J. Atmos. Sci.*, 48: 1,238-1,248.
- [8] Neelin, J. D. and F.-F. Jin, 1993: Models of inter-annual tropical ocean-atmosphere interaction - a unified view. part ii: analytical results in the weak-coupling limit. *J. Atmos. Sci.*, 50: 3,504-3,522.
- [9] Penland, C. and P. D. Sardeshmukh, 1995: The optimal-growth of tropical sea-surface temperature anomalies. *J. of Climate*, 8: 1,999,024.
- [10] Suarez, M. J., and P. S. Schopf 1988: A delayed action oscillator for ENSO, *J. Atmos. Sci.*, 45, 3283-3287.
- [11] Tziperman, E., L. Stone, M. A. Cane and H. Jarosh, 1994: El Niño Chaos: Overlapping of resonances between the seasonal cycle and the Pacific Ocean-Atmosphere oscillator. *Science*, 264, 72-74.

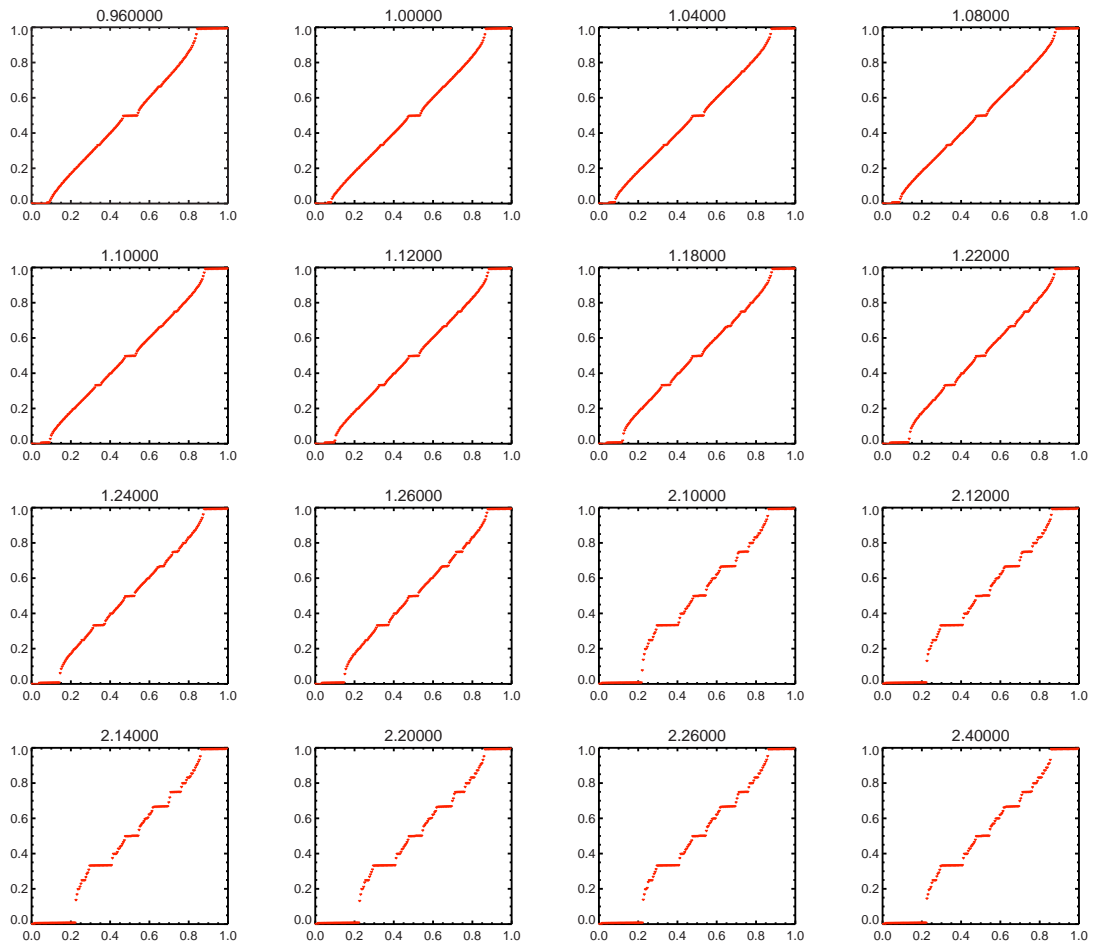


FIG. 16: AllRunsWINDINGSpec.ps.

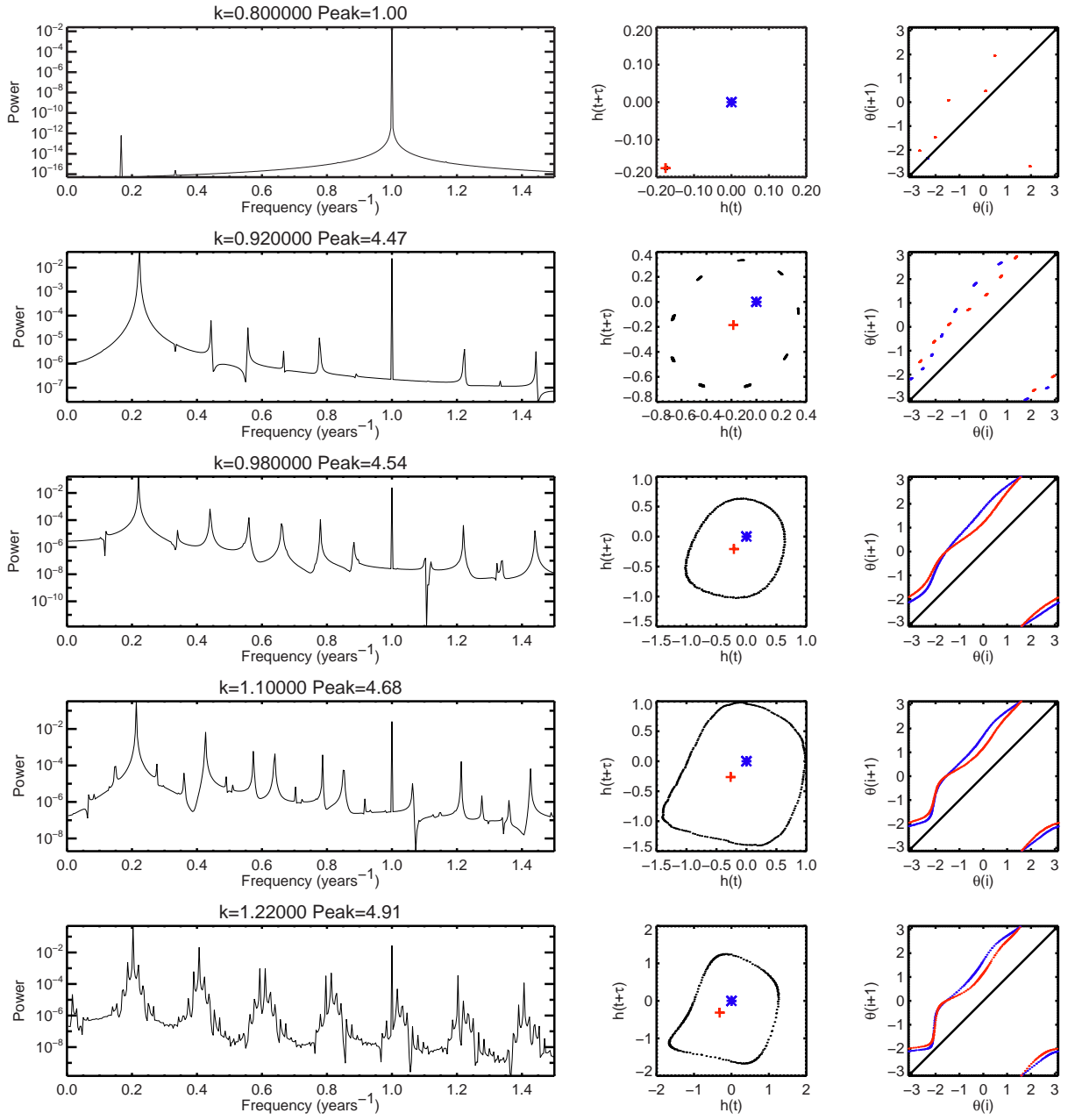


FIG. 17: Similar as Figure 8 including generation of Kelvin waves due to MJO.

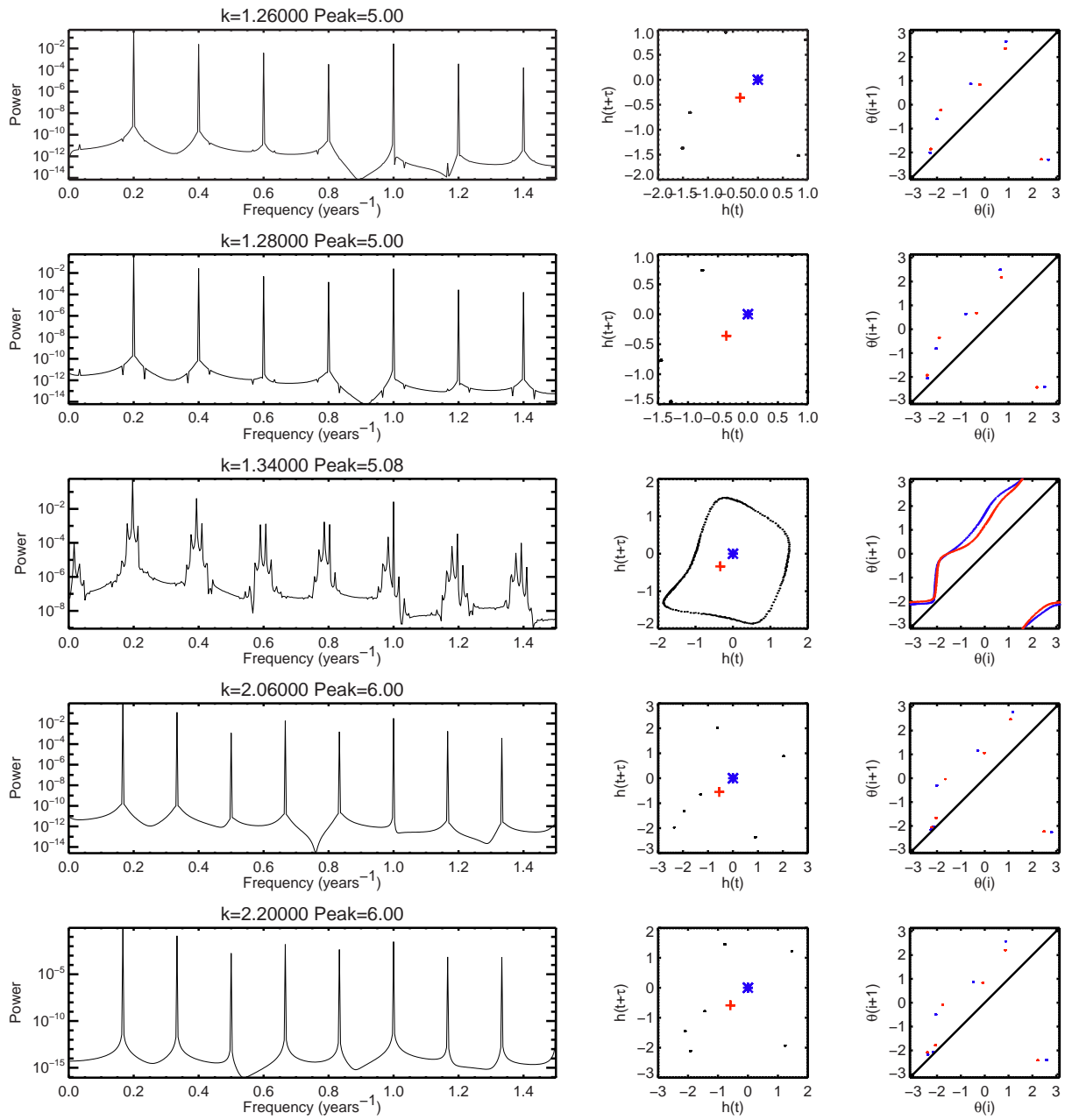


FIG. 18: Continuation of Figure 17